Published in final edited form as:
Anal Chem. 2009 November 15; 81(22): 9499–9506. doi:10.1021/ac902006p.

Label-Free Quantitation of a Cancer Biomarker in Complex Media using Silicon Photonic Microring Resonators

Adam L. Washburn[†], **L. Cary Gunn**[‡], and **Ryan C. Bailey**[†,*]

[†]Department of Chemistry, Institute for Genomic Biology, and Micro and Nanotechnology Laboratory, University of Illinois at Urbana-Champaign, 600 South Mathews Avenue, Urbana, Illinois 61801

[‡]Genalyte, Inc., 11760 Sorrento Valley Road, Suite R, San Diego, CA 92121

Abstract

Recent advances in label-free biosensing techniques have shown the potential to simplify clinical analyses. With this motivation in mind, this paper demonstrates for the first time the use of silicon-on-insulator microring optical resonator arrays for the robust and label-free detection of a clinically important protein biomarker in undiluted serum, using carcinoembryonic antigen (CEA) as the test case. We utilize an initial slope-based quantitation method to sensitively detect CEA at clinically relevant levels and determine the CEA concentrations of unknown samples in both buffer and undiluted fetal bovine serum. Comparison with a commercial enzyme-linked immunosorbent assay (ELISA) kit reveals that the label-free microring sensor platform has a comparable limit of detection (2 ng/mL) and superior accuracy in the measurement of CEA concentration across a three order of magnitude dynamic range. Notably, we report the lowest limit of detection to date for a microring resonator sensor applied to a clinically relevant cancer biomarker. Although this report describes the robust biosensing capabilities of silicon photonic microring resonator arrays for a single parameter assay, future work will focus on utilizing the platform for highly multiplexed, label-free bioanalysis.

Introduction

Fluorescent,[1] nanoparticle,[2] or enzymatic labels[3] are utilized in many common biomolecular assays and can provide exceptional sensitivity down to the single molecule level. However, they may also introduce challenges in terms of cost, complexity, labeling heterogeneity,[4] and perturbations to the native biomolecular interaction of interest.[5] For these reasons, the development of label-free approaches for bioanalysis, especially those that can measure multiple analytes simultaneously, has been an active area of research over the past 20 years.[6] Particularly relevant to this report are optical methods of label-free analysis,[7] including surface plasmon resonance,[8] photonic crystals,[9] and interferometric devices,[10] which have all been utilized to sensitively detect biomolecules as well as determine binding kinetics.

High quality factor (Q factor) microcavity resonators represent a promising class of optical devices that have only recently been utilized for biomolecular analysis.[11, 12] In microcavity resonator sensors, which include microspheres,[13–15] microtoroids,[16] capillaries,[17–21] microdisks,[22,23] and microrings,[24–30] light is coupled into the cavity via an adjacent linear

---

*baileyrc@illinois.edu.

Supporting Information Available: Representative surface functionalization results and detailed descriptions of the data-fitting procedures utilized in this work are available in the supporting information. This material is available free of charge via the Internet at http://pubs.acs.org.

waveguide positioned within the evanescent field. Optical modes are supported along the circumference of the cavity according to the resonance condition:

$$m\lambda=2\pi r n_{\mathrm{eff}} \tag{1}$$

where m is an integer, λ is wavelength of light, r is the radius of the resonator, and n_{eff} is the effective refractive index. Precise fabrication leads to high Q factor cavities which, from a practical analytical standpoint, lead to a dramatic increase in the effective optical pathlength as well as a sharpening of the resonance to an extraordinarily narrow spectral dispersion. Chemical and biomolecular binding events at the surface of the microcavity lead to an increase in the effective refractive index, n_{eff}, and thus a shift in the resonance frequency, as shown in Figure 1A. The narrow resonance allows resolution of small shifts, and thus tiny binding-induced changes in n_{eff}, can be clearly discerned, directly facilitating highly sensitive detection.

Silicon-on-insulator (SOI) optical microring resonators are an attractive technology for applications in label-free biomolecular analysis holding significant promise for multiplexed biomolecular detection. Since both the ring and waveguide are physically anchored to the same underlying substrate (see SEM image in Figure 1B), these devices can be routinely fabricated using well-characterized semiconductor processing techniques and easily interrogated via chip-integrated optics.

Prior reports of optical microring resonators for protein sensing have generally focused on proof-of-principle demonstrations, such as measurements in buffer of avidin-biotin interactions[25–29] or detection of polyclonal IgG.[30] Besides demonstrating the ability to monitor in real time the steps involved in the chemical and biomolecular functionalization of the sensor surface, we also utilize multiple types of integrated on-chip control sensors for nonspecific response normalization and implement a time-based quantitation method that enables rapid calibration and precise concentration determination. As a demonstration of the impact of these features, we focus on the direct and label-free quantitation of carcinoembryonic antigen (CEA), a 185 kDa glycoprotein that is secreted into the blood and has been established as a biomarker for many human cancers, including colorectal,[31] cervical,[32] lung,[33] and breast[34] cancers. We show that the detection limit of our platform is comparable to that of a commercial enzyme-linked immunosorbent assay (ELISA) kit and is satisfactory for the quantitation of CEA over the clinically-relevant range of 5–100 ng/mL. We also report for the first time operation of microring optical resonators in undiluted fetal bovine serum and show that CEA can be detected in this complex medium at concentrations found in patients with advanced cancers, from 20 to well over 70 ng/mL.[35] This report establishes microring resonator arrays as a promising tool for a variety of real-world protein detection applications.

Experimental Section

Materials

The silane, 3-aminopropyltriethoxysilane (APTES), was purchased from Gelest (Morrisville, PA). Succinimidyl 6-hydrazinonicotinamide acetone hydrazone (S-HyNic) and succinimidyl 4-formylbenzoate (S-4FB) were purchased from SoluLink (San Diego, CA). Monoclonal mouse antibody to human CEA (Cat# M37401M) and human CEA (Cat# A32030H) were purchased from Meridian Life Science (Saco, ME). CEA ELISA kits were purchased from GenWay Biotech (San Diego, CA) and Signosis (Sunnyvale, CA). Fetal bovine serum (FBS) was purchased from Gemini Bio-Products (West Sacramento, CA). Zeba spin filter columns were purchased from Pierce (Rockford, IL). PBS was reconstituted from Dulbecco's Phosphate Buffered Saline packets purchased from Sigma-Aldrich (St. Louis, MO). All other chemicals were obtained from Sigma-Aldrich and used as received.

All buffers were made with purified water (ELGA PURELAB filtration system; Lane End, UK), and the pH was adjusted using 1 M HCl or 1 M NaOH. PBS pH 7.4. Acetate buffer consisted of 50 mM sodium acetate and 150 mM sodium chloride adjusted to pH 4.75. Glycine buffer was 10 mM glycine and 160 mM NaCl adjusted to pH 2.2. BSA-PBS buffer was made by dissolving solid bovine serum albumin (BSA) in PBS (pH 7.4) to a final concentration of 0.1 mg/mL.

Substrate Design, Fabrication, and Sensor Chip Layout

Microring resonator array substrates were designed as previously described[36, 37] and fabricated on 8" silicon-on-insulator (SOI, 200 nm thick top-layer Si) wafers by the silicon foundry at LETI (Grenoble, France). The entire 8" wafer was spin-coated with a commercially-available perfluoro (alkenyl vinyl ether) copolymer (Asahi Glass Company), and windows were opened over selected individual sensor elements via photolithography and reactive ion etching. Individual sensor chips having sixty-four 30 μm diameter microrings on a 6 × 6 mm footprint were diced from the 8" wafers by Grinding and Dicing Services, Inc. (San Jose, CA). Next to each microring was a linear waveguide that had input and output diffractive grating couplers at either end, allowing the optical cavity spectrum of each microring resonator to be determined independently.

Instrumentation

The instrumentation used to measure shifts in microring resonance frequency is described in detail in a separate manuscript.[37] Briefly, the beam of a tunable, external cavity diode laser operating with a center frequency of 1560 nm is rapidly rastered across the surface and the back reflection is monitored as a function of position to image the substrate. This image is used to register the location of the input and output grating couplers associated with each individual microring. To determine the resonance frequency of an individual microring, the beam is focused onto a single input grating coupler. The intensity of light projected off of the chip by the corresponding output grating coupler is measured as the frequency of the laser is rapidly swept through a suitable spectral bandwidth. In this mode of operation, a resonance appears as a decrease in the intensity of light projected out of the output coupler at a given laser frequency, since under resonance conditions light is nearly completely coupled into the microring and no longer propagates down the adjacent linear waveguide. Resonance frequencies and shifts in frequency are determined and displayed on-screen in near real time with up to ~250 ms resolution using the provided instrument control software. Multiple resonator sensors in an array are probed by serially positioning the laser beam on different input grating couplers that address unique microrings and then the resonance frequency is recorded as described above. Up to 32 microring sensors can be monitored during an experiment. Eight of the sensors monitored are not exposed to the solution and serve as controls for thermal drift.

Sensor chips are loaded into a custom cell with microfluidic flow channels defined by a 0.010" thick laser-cut Mylar gasket (fabricated by RMS Laser; El Cajon, CA) that is aligned over top of the microring arrays and sandwiched between an aluminum chip holder and a Teflon lid (see supplementary Figure S-1 for a diagram of the microring layout, including an overlay of the Mylar gasket). Solutions are introduced to the chip at controlled flow rates using an 11 Plus syringe pump (from Harvard Apparatus; Holliston, MA) operated in withdraw mode.

Surface Functionalization and Biomolecule Attachment

To remove any residual organic contaminants remaining from fabrication, silicon microring surfaces are first cleaned by a one-minute immersion in piranha solution[38] (3:1 H_2SO_4:30% H_2O_2) and are then rinsed with copious amounts of water and dried under a stream of nitrogen. Following cleaning, the silicon microrings are then organically modified using standard silanization chemistry. The entire chip is exposed to a 2% solution of APTES in 95% ethanol for 10–20 min, followed by a removal of residual siloxane by rinsing in 95% ethanol. Covalent attachment of biomolecules to the sensor surface is achieved in two steps using hydrazone-bond-formation chemistry. The freshly silanized surfaces are exposed to a 17 mM solution of S-HyNic in PBS (with 4% dimethylformamide (DMF) to dissolve SHyNic) for 3–4 h. In parallel, a reactive aldehyde moiety is conjugated to the antibody (1 mg/mL) by reaction with a 5-fold molar excess of S-4FB (dissolved first in DMF and diluted in PBS to less than 5% DMF). This S-4FB:protein ratio introduces an average of two pendant reactive aldehyde groups per antibody, according to the manufacturer, and was empirically determined to be optimal. After reacting for 2 h at room temperature, unreacted S-4FB is removed by buffer-exchanging the antibody into acetate buffer using Zeba spin filter columns. HyNic-functionalized surfaces are exposed to solutions of 4FB-functionalized antibodies (generally 0.1 mg/mL or higher) for at least 1 h to maximize the amount of covalently immobilized antibody. A glycine buffer rinse is then used to remove noncovalently bound antibody. A final blocking step is accomplished by exposing the sensor surface to a 2% solution (w/w) of BSA in PBS. In a typical assay, half of the sensor rings are functionalized with antibody while the other half are not exposed to antibody. These nonfunctionalized sensors are used as internal references to correct for temperature and instrument drift, as well as for bulk refractive index shifts associated with switching solutions.

All silanization and HyNic conjugation reactions, as well as detection experiments, are performed in linear microfluidic channels defined by the Mylar gasket. For experiments in which antibodies are immobilized only onto certain regions of the substrate, a different Mylar gasket is used that directs fluid to only selected portions of the sensor chip. While microfluidics alone provide adequate spatial resolution for the measurements in this paper, preliminary work in our group has indicated that higher order multiplexing can be achieved by interfacing with conventional microarray spotting technologies.

CEA Detection

For CEA detection experiments in buffer, BSA-PBS (0.1 mg/mL BSA in PBS) was used as a running buffer to help prevent nonspecific adsorption of protein in the tubing and flow cell. CEA solutions were made by serial dilution in BSA-PBS starting from an original 2.5 mg/mL stock solution. Those solutions were then flowed through the sample chamber and over the sensor chip surface at a rate of 30 μL/min. For CEA detection in serum, 100% FBS was used as a running buffer. To detect CEA in serum, CEA-spiked FBS samples were made by adding CEA stock solution to 100% FBS. Additional solutions were made by directly diluting the CEA-spiked FBS stock solution with 100% FBS to dilute the CEA to the appropriate concentration. Because of the viscosity of 100% FBS, the flow rate was reduced to 10 μL/min for sensing experiments in serum. For all of the sensing assays, the original surfaces were regenerated after CEA exposure using a 1–2 minute rinse of glycine buffer that disrupted protein-antibody complexes, followed by a return to the running buffer to reestablish the sensor baseline. Single-blind solutions having unknown CEA concentrations were generated—by a laboratory worker otherwise not involved in this study—by adding an aliquot of an original stock solution into either BSA-PBS buffer or 100% FBS.

For the CEA ELISA, absorbance was measured at 450 nm using a SpectraMax Plus384 spectrophotometer from (Molecular Devices; Sunnyvale, CA).

Data Processing

All microring detection data was corrected for drift related to thermal and instrumental fluctuations, as well as minimal amounts of non-specific binding by referencing to “unmodified” rings that were exposed to solution in the same sample flow chamber but were masked during the antibody immobilization step. Graphs of sensor responses have been processed post-acquisition by subtracting the unmodified reference ring responses from the antibody-conjugated sensor rings. All data fitting was performed using the OriginPro 8 software package (OriginLab Corporation; Northampton, MA).

Results and Discussion

Surface Derivatization of Microring Resonator Surface

For sensitive detection of biomolecules, a robust capture agent immobilization strategy is needed. Figure 2 schematically outlines the multiple steps used to covalently attach antibodies to the silicon surface of a microring sensor. As shown in Figures 2A and 2B, the oxide-passivated silicon surface is first modified with 3-aminopropyltriethoxysilane (APTES). Because addition of organic molecules and biomolecules to the sensor surface changes the local refractive index, each surface reaction can be monitored in real time. Figure 3A shows the real-time response of twelve individual microrings simultaneously exposed to a 2% solution of APTES. Following addition of the silane, an immediate shift in resonance frequency is observed that contains contributions from the bulk refractive index change associated with the 2% APTES as well as from rapid surface silanization. As the sensors are rinsed with 95% EtOH and returned to the original bulk refractive index environment, the sensors decrease in signal but a residual shift in the resonance wavelength of approximately 75 pm indicates the covalent attachment of APTES to the surface.

As indicated by the schematic in Figure 2C, the amine-reactive succinimidyl 6-hydrazinonicotinamide acetone hydrazone (S-HyNic) is added to the APTES-functionalized surface (Figure S-2 in the Supporting Information shows the real-time response as HyNic is attached to APTES-modified microrings). The hydrazine-presenting surface then enables antibodies tagged with succinimidyl 4-formylbenzoate (S-4FB) to be covalently coupled to the surface via hydrazone bond formation between the aryl aldehydes on the antibodies and the hydrazine moieties on the surface, as illustrated in Figure 2D. Figure 3B shows the real-time data for the addition of 4FB-tagged anti-CEA antibodies to five identical HyNic-modified microrings resulting in a 300–350 pm shift in the resonance frequencies of each ring. A rinse with glycine buffer helps remove any noncovalently bound antibody, and after returning to the original acetate buffer, the remaining 260–280 pm shift for each ring corresponds to antibody attached to the microring surface via a hydrazone bond linkage.

By monitoring each surface derivatization step, it is possible to verify that each individual chemical modification of the surface has occurred. In addition, it is possible to determine the sensor-to-sensor consistency of antibody loading. Since inconsistency in antibody loading is a common source of assay variability, this is a very significant feature of our detection system that will be critical for future work in the creation of robust and reproducible multiplexed sensor arrays.

Following the immobilization of anti-CEA antibodies, microring sensors were tested to verify that the immobilized antibody was still functional and that the sensors were responsive to antigen binding. Figure 4 shows the uncorrected (no control ring subtraction) response of anti-CEA functionalized microrings to a 1 μg/mL solution of CEA in BSA-PBS at $t = 5$ min, followed by regeneration with glycine buffer at $t = 12$ min with a return to BSA-PBS at $t = 14$ min. The exposure to CEA induces a specific response from five individual antibody-functionalized microrings, each displaying a net frequency shift of ~100 pm after 7 min of binding. Notably, the relative response of each of the rings is extremely similar, consistent with the observed antibody loading shown in Figure 3B. Also shown in Figure 4 are the responses of five individual control rings that are in the same channel as the five rings that showed a specific response. These microrings are identical except that they were not exposed to the 4FBtagged antibody solution, and they showed no response during the same exposure to antigen. Thus, for all following biomolecular binding/detection experiments performed in this paper (shown in Figure 4–Figure 6), these unmodified rings are used as references. An important advantage of using an array of microring sensors is that unmodified rings can be used as reference rings in order to subtract out any systematic instrumental or thermal drift, as well as to remove sensor response caused by a change in the bulk refractive index or from small amounts of nonspecific binding.

Quantitative Detection of a Cancer Biomarker

To make quantitative measurements of CEA, microring resonators were covalently functionalized with anti-CEA antibodies as described. To demonstrate the dynamic range for this sensing technique, aliquots of CEA were sequentially flowed over the sensor array at concentrations of 45, 114, 228, 575, and 1183 ng/mL in BSA-PBS, and the shift in resonance frequencies of several microrings were monitored in real-time. At each concentration, the CEA solution was flowed for 25 minutes of binding followed by a quick (1–2 minute) rinse with glycine to regenerate the original antibody-presenting sensor surface and a 5–10 minute rinse with BSA-PBS to reestablish the baseline. Figure 5 shows a representative response from a single microring (only one shown for clarity) during the entire concentration exposure series. This dose and regeneration protocol was repeated three times in order to obtain all association curves in triplicate for post-acquisition data analysis.

To demonstrate the consistency of the observed CEA detection response, the data from a single microring during each of the three concentration series runs was overlaid, as shown in Figure 6A. The good agreement in both the magnitude and shape of the association curves allows CEA concentration determination with high precision. From the data in Figure 6A, a calibration curve was generated based upon the initial slopes of the association curves. As described by Fick's first law, under the mass-transport limiting conditions usually present in trace biomolecular analysis, the initial slope is linearly proportional to the concentration of the analyte in solution.[39] The resulting concentration-response calibration curve is generally linear over a wide dynamic range, and thus the method is advantageous for real-time detection assays.[30, 40–42] In addition, we have found that using an initial slope-based method provides increased precision as compared to fixed-time-point measurements for the 10-minute assays described in this paper. This increased precision is largely because the initial slope is determined from multiple data points over a given time range, whereas equilibrium-based measurements typically measure the response at a single time point, or over a discrete time range, during which the response is growing. For our system, multiple measurements based on initial slope typically have standard deviations about 3–6 times smaller than the standard deviations based on multiple measurements using a fixed time point.

In order to accomplish this analysis, the initial portion of the association curve is fit to an exponential functional form and then differentiated at $t = 0$ to give the initial slope (a more detailed description of the data fitting and initial slope determination can be found in the Supporting Information). The colored lines in Figure 6A represent fitted tangent lines that give the initial slope for each association curve at each concentration. The initial slope values determined from the data in Figure 6A are plotted as a function of concentration in Figure 6B (error bars 95% confidence interval (C.I.), number of measurements (n) = 3). Notably, the resulting slope-based calibration plot is linear (coefficient of determination (R^2) for the linear fit is 0.997), which enables simple sensor calibration and extended linear dynamic range, particularly at higher antigen concentrations. While data from only a single microring is shown for clarity, the response of multiple sensors were simultaneously recorded and found to also yield linear calibration plots with extended dynamic ranges. While each microring behaved in a similar fashion, it is apparent that small differences in antibody loading require each microring sensor to be independently calibrated. Methods of *a priori* sensor normalization are currently being investigated; however, the process of independent calibration has the potential to be fully automated in future applications.

To demonstrate the ability of microring sensors to quantify samples containing lower concentrations of CEA, a second calibration curve was constructed based on the initial slope approach using standard concentrations from 0 to 121 ng/mL—encompassing the clinically-relevant range of 5–100 ng/mL. The initial slope-based concentration response curve is shown in Figure 6C (error bars 95% C.I., n = 3). Again a linear calibration plot is observed ($R^2 = 0.997$). The real-time association data shown in Figures 6B and 6C were obtained with the same microring, but on different days. While the slopes of the calibration traces are similar, they are not identical, and there is a noticeable difference in the y-intercept—largely due to the variation in the dynamic range of each calibration plot. This observation reinforces the notion that at this stage each sensor must be independently calibrated on the same day and, ideally, calibrated directly in series with unknown samples. As with any calibration curve, the greatest accuracy for evaluating an unknown will be obtained by using calibration concentrations within a relevant range for the unknowns.

While the generation of calibration curves from standards is important, the obvious objective is the quantitation of unknown samples of CEA. Two blinded unknown samples A and B were measured to determine the concentrations of CEA using both a microring sensor and a commercial CEA ELISA kit. Both unknown solutions were flowed over the microring in triplicate, interspersed between the three concentration series runs used to generate the calibration curve in Figure 6C. The initial slopes were determined for the lower concentration CEA standards and for the unknowns. The unknown samples had slopes of 1.7 pm/min and 0.36 pm/min for unknowns A and B, respectively. Figure 6C shows the mapping of these initial slope values onto the calibration curve and quantitation of the unknowns as 90 ± 2 and 18 ± 1 ng/mL, respectively (uncertainties are based on the 95% C.I. for a calibration curve with n = 18, with three replicate unknown evaluations). The concentration values were then compared with those obtained using a commercial ELISA kit. The same unknown solutions (A and B) were assayed in a 96-well plate along with the provided standards according to manufacturer instructions. Concentration determination via ELISA gave concentrations of 112 ± 11 and 17 ± 9 ng/mL for unknowns A and B, respectively (uncertainties are based on the 95% C.I. for the ELISA calibration curve with n = 18, with three replicate unknown evaluations).

Following quantitation of CEA via both microring sensors and the commercial ELISA kit, the concentrations of the prepared blinded unknowns A and B were revealed to be 91 and 17 ng/mL, respectively. Interestingly, both microrings and ELISA were able to determine the lower concentration with a high degree of accuracy. Unknown A, which is higher in concentration, was also correctly determined via the microring resonators. However, the “correct” value falls outside the 95% confidence interval for the ELISA assay. Notably, the 95% confidence intervals are considerably larger for the ELISA assay. At higher concentrations this is likely due to the larger absorbance values that test the linearity of the spectrometer. The error in high concentration determination might be reduced by shortening the time of the development step, but this would compromise the ability to accurately quantitate at lower concentrations. This trade-off in the quantitative ability of ELISA across a one order of magnitude dynamic range is clearly less of a concern using the label-free microring resonator sensor.

To determine a detection limit for the microring resonator sensor, a minimum resolvable change in initial slope must be established in comparison to the normal baseline “slope noise.” To achieve this, the standard deviation of the linear slope (slope noise, σ) of representative 7 min baseline sections (the same period of time over which the initial slope was fit for determination of low antigen concentrations) was measured to be 0.02 pm/min. Extrapolating to the 3σ

threshold, the limit of detection for CEA in BSA-PBS was determined to be ~2 ng/mL. Notably, this value is below the basal levels (3–5 ng/mL) of CEA present in the serum of "healthy" adults. The microring detection limit is also comparable to the stated manufacturer value for the commercial ELISA kit of 1 ng/mL. Notably, the initial slope-based concentration determination can be accomplished in less than 30 minutes using microring resonators—a total of four 7 min runs (three standards and one unknown sample)—which is significantly faster than the 3+ hour ELISA procedure. Given the favorable precision, similar limit of detection, and assay speed in comparison to an ELISA assay, the potential of microring resonators for rigorous quantitation of unknown protein concentrations is high.

By way of comparison, multiple microring sensors on a given chip are observed to vary in the slope of the calibration curve slope by about 10–20%. However, the precision of each calibration curve remains fairly consistent, allowing unknowns to be evaluated among multiple sensors with a standard deviation of around 1–2 ng/mL, on the same magnitude as the observed uncertainty for a single calibration curve.

Cancer Biomarker Detection in Serum

We have also evaluated the ability of microring sensors to detect CEA in 100% fetal bovine serum. By adding human CEA to FBS, the detection platform was challenged with a complex sample matrix similar to that encountered when analyzing human serum or other biological fluids. CEA standards were created in FBS at concentrations of 0, 19, 49, 98, and 199 ng/mL, and the analysis was performed on a sensor chip functionalized with an anti-CEA antibody. As with CEA detection in buffer, the concentration of CEA in FBS was directly related to the initial slope following addition of the samples. However, because FBS contains a high concentration of proteins that nonspecifically adsorb to the sensor surface, addition of FBS resulted in a drifting baseline signal that could only be partially corrected using the on-chip control rings, as can be seen from an example trace in Figure 7A. Therefore, to accurately determine the sensor response to CEA, the slope of the baseline was measured 5 min before injection of the CEA sample and the slope of the drifting baseline was subtracted from the measured slope after the injection time (see Table S-3 in Supporting Information for information on baseline slopes and CEA-response slopes for all of the calibration series). To test the validity of the calibration curve, a blinded unknown was evaluated and determined to have a concentration of 61 ± 23 ng/mL by comparison with the standard calibration curve shown in Figure 7B (uncertainties for unknowns are based on the 95% C.I. for a calibration curve with n = 15, unknown run one time). The microring resonator results were again correlated with those of a commercially-available ELISA, which gave a value of 67 ± 9 ng/mL (see Supporting Information). Both values were in good agreement with the prepared unknown concentration of 70 ng/mL, as revealed by analyses using microring and ELISA methods.

By comparing the slopes of the calibration curves for microring resonator detection of CEA in both buffer and serum, it is apparent that sensitivity is greatly reduced in serum. Whereas detection in buffer gives a slope of 0.019 (pm/min)/(ng/mL), see Figure 6C, detection in serum shows a ~6 fold decrease to 0.0036 (pm/min)/(ng/mL), as shown in Figure 7. This is not unexpected, however, since the specific binding of CEA is in competition for available antibody recognition sites with nonspecific interactions from serum proteins, some of which are present at 10^8-fold higher concentration.[43] In addition, the baseline "slope noise" in serum (determined in the same manner as for detection in buffer) was found to be 0.03 pm/min, which is slightly larger than the 0.02 pm/min for detection in buffer. This increased slope noise is largely the result of nonspecific serum adsorption that causes the drifting baseline, which, although largely linear, does have a slowly decreasing slope over time. While this nonlinear behavior limits the precision of slope determination it does not preclude quantitation of CEA levels in an unknown sample. Taken together, the decreased sensitivity to CEA in serum (as compared to buffer) and the slightly increased baseline noise result in a limit of detection of 25 ng/mL. Although still within the range monitored clinically (5–100 ng/mL), future work to lower the detection limit and improve measurement precision in serum will be necessary. One area of particular focus is minimizing nonspecific serum protein adsorption through improved surface treatment.

Conclusion

In this paper we establish that arrays of silicon photonic optical microring resonators are a robust emerging tool for bioanalysis of clinically relevant samples. We show the ability to directly visualize the chemical and biochemical functionalization of the sensor surface to ensure consistent loading of antibody capture agents. We then demonstrate the applicability of the microring resonator platform for the sensitive and robust detection of a relevant marker of disease at clinically relevant levels in both buffer and fetal bovine serum. By utilizing a quantitation scheme based upon measuring the time-resolved initial slope of the sensor response, the concentration of unknown CEA solutions in buffer are determined in a label-free format with comparable sensitivity and improved precision over commercial ELISA assays. The established limits of detection are among the lowest ever reported for microring resonators applied to protein detection. We also demonstrate the first-ever operation of such a device in undiluted serum. While still at an early stage of development, the inherent multiplexing capability of this optical semiconductor-based analysis technology, coupled with the detection limits and precision demonstrated herein, establishes silicon-on-insulator microring resonators as a promising platform for highly multiplexed, label-free biomolecular analysis.

Supplementary Material

Refer to Web version on PubMed Central for supplementary material.

Acknowledgments

This work was funded by the NIH Director's New Innovator Award Program, part of the NIH Roadmap for Medical Research, through grant number 1-DP2-OD002190-01 and the Camille and Henry Dreyfus Foundation. ALW is supported via a National Science Foundation Graduate Research Fellowship. We acknowledge Matthew Luchansky for his assistance in creating the unknown CEA solutions and Ji-Yeon Byeon for the SEM image of the microring resonator. This research was carried out in part in the Frederick Seitz Materials Research Laboratory Central Facilities, University of Illinois, which are partially supported by the U.S. Department of Energy under grants DE-FG02-07ER46453 and DE-FG02-07ER46471.

References

1. Royer, CA.; Scarlata, SF.; Ludwig, B.; Michael, LJ. Methods in Enzymology. Vol. Vol. Volume 450. Academic Press; 2008. p. 79-106.
2. Seydack M. Biosensors and Bioelectronics 2005;20:2454–2469. [PubMed: 15854819]
3. Hempen C, Karst U. Analytical & Bioanalytical Chemistry 2006;384:572–583. [PubMed: 16208465]
4. Kodadek T. Chemistry & Biology 2001;8:105–115. [PubMed: 11251285]
5. Sun YS, Landry JP, Fei YY, Zhu XD, Luo JT, Wang XB, Lam KS. Langmuir 2008;24:13399–13405. [PubMed: 18991423]
6. Qavi AJ, Washburn AL, Byeon J-Y, Bailey RC. Anal Bioanal Chem 2009;394:121–135. [PubMed: 19221722]
7. Fan X, White IM, Shopoua SI, Zhu H, Suter JD, Sun Y. Analytica Chimica Acta 2008;620:8–26. [PubMed: 18558119]
8. Homola J. Chem. Rev 2008;108:462–493. [PubMed: 18229953]
9. Cunningham BT, Laing L. Expert Review of Proteomics 2006;3:271–281. [PubMed: 16771700]

10. Gauglitz G, Proll G. Adv. Biochem. Eng./Biotechnol 2008;109:395–432.
11. Vollmer F, Arnold S. Nat. Methods 2008;5:591–596. [PubMed: 18587317]
12. Jokerst, Nan; Royal, Matthew; Palit, Sabarni; Luan, Lin; Dhar, Sulochana; Tyler, Talmage. Journal of Biophotonics 2009;2:212–226. [PubMed: 19367589]
13. Ren HC, Vollmer F, Arnold S, Libchaber A. Opt. Express 2007;15:17410–17423. [PubMed: 19551035]
14. Vollmer F, Arnold S, Braun D, Teraoka I, Libchaber A. Biophysical Journal 2003;85:1974–1979. [PubMed: 12944310]
15. Vollmer F, Braun D, Libchaber A, Khoshsima M, Teraoka I, Arnold S. Applied Physics Letters 2002;80:4057–4059.
16. Armani AM, Kulkarni RP, Fraser SE, Flagan RC, Vahala KJ. Sci 2007;317:783–787.
17. Suter JD, White IM, Zhu H, Shi H, Caldwell CW, Fan X. Biosensors and Bioelectronics 2008;23:1003–1009. [PubMed: 18036809]
18. White IM, Oveys H, Fan X, Smith TL, Zhang J. Applied Physics Letters 2006;89
19. Zhu H, White IM, Suter JD, Dale PS, Fan X. Opt. Express 2007;15:9139–9146. [PubMed: 19547254]
20. Zhu H, White IM, Suter JD, Zourob M, Fan X. Analyst 2008;133:356–360. [PubMed: 18299750]
21. Zhu HY, White IM, Suter JD, Fan XD. Biosensors & Bioelectronics 2008;24:461–466. [PubMed: 18550355]
22. Boyd RW, Heebner JE. Applied Optics 2001;40:5742–5747. [PubMed: 18364865]
23. Krioukov E, Klunder DJW, Driessen A, Greve J, Otto C. Optics Letters 2002;27:512–514. [PubMed: 18007849]
24. Chao CY, Guo LJ. Applied Physics Letters 2003;83:1527–1529.
25. Xu DX, Densmore A, Delâge A, Waldron P, McKinnon R, Janz S, Lapointe J, Lopinski G, Mischki T, Post E, Cheben P, Schmid JH. Opt. Express 2008;16:15137–15148. [PubMed: 18795053]
26. Chao CY, Fung W, Guo LJ. IEEE Journal of Selected Topics in Quantum Electronics 2006;12:134–142.
27. De Vos KM, Bartolozzi I, Bienstman P, Baets R, Schacht E. 20072007
28. Yalcin A, Popat KC, Aldridge JC, Desai TA, Hryniewicz J, Chbouki N, Little BE, King O, Van V, Chu S, Gill D, Anthes-Washburn M, Unlu MS. IEEE Journal of Selected Topics in Quantum Electronics 2006;12:148–155.
29. De Vos K, Girones J, Popelka S, Schacht E, Baets R, Bienstman P. Biosensors and Bioelectronics 2009;24:2528–2533. [PubMed: 19200711]
30. Ramachandran A, Wang S, Clarke J, Ja SJ, Goad D, Wald L, Flood EM, Knobbe E, Hryniewicz JV, Chu ST, Gill D, Chen W, King O, Little BE. Biosensors and Bioelectronics 2008;23:939–944. [PubMed: 17964774]
31. Wang JY, Tang RP, Chiang JM. Diseases of the Colon & Rectum 1994;37:272–277. [PubMed: 8137675]
32. Borras G, Molina R, Xercavins J, Ballesta A, Iglesias J. Gynecologic oncology 1995;57:205–211. [PubMed: 7729735]
33. Sung H-J, Cho J-Y. BMB Reports 2008;41:615–625. [PubMed: 18823584]
34. Sölétormos G, Nielsen D, Schiøler V, Mouridsen H, Dombernowsky P. European Journal of Cancer 2004;40:481–486. [PubMed: 14962712]
35. Schiemann U, Gunther S, Gross M, Henke G, Muller-Kock Y, Konig A, Munders M, Folwaczny C, Mussack T, Holinski-Feder E. Cancer Detection and Prevention 2005;29:356–360. [PubMed: 16122885]
36. Bailey RC, Washburn AL, Qavi AJ, Iqbal M, Gleeson M, Tybor F, Gunn LC. Proc. SPIE 2009;7220:72200N.
37. Iqbal M, Gleeson M, Tybor F, Spaugh B, Gunn W, Hochberg M, Baehr-Jones T, Bailey RC, Gunn LC. J. Sel. Topics. Quant. Elect. 2009in press
38. Daimon M, Masumura A. Appl. Opt 2007;46:3811–3820. [PubMed: 17538678]
39. Eddowes MJ. Biosensors 198788;3:1–15. [PubMed: 3675654]

40. Tunnemann R, Mehlmann M, Sussmuth RD, Buhler B, Pelzer S, Wohlleben W, Fiedler H-P, Wiesmuller K-H, Gauglitz G, Jung G. Analytical Chemistry 2001;73:4313–4318. [PubMed: 11569825]

41. Adamczyk M, Mattingly PG, Shreder K, Yu Z. Bioconjugate Chemistry 1999;10:1032–1037. [PubMed: 10563772]

42. Cheng T-J, Lin T-M, Chang H-C. Analytica Chimica Acta 2002;462:261–273.

43. Anderson NL, Anderson NG. Molec. Cell. Proteomics 2002;1:845–867. [PubMed: 12488461]

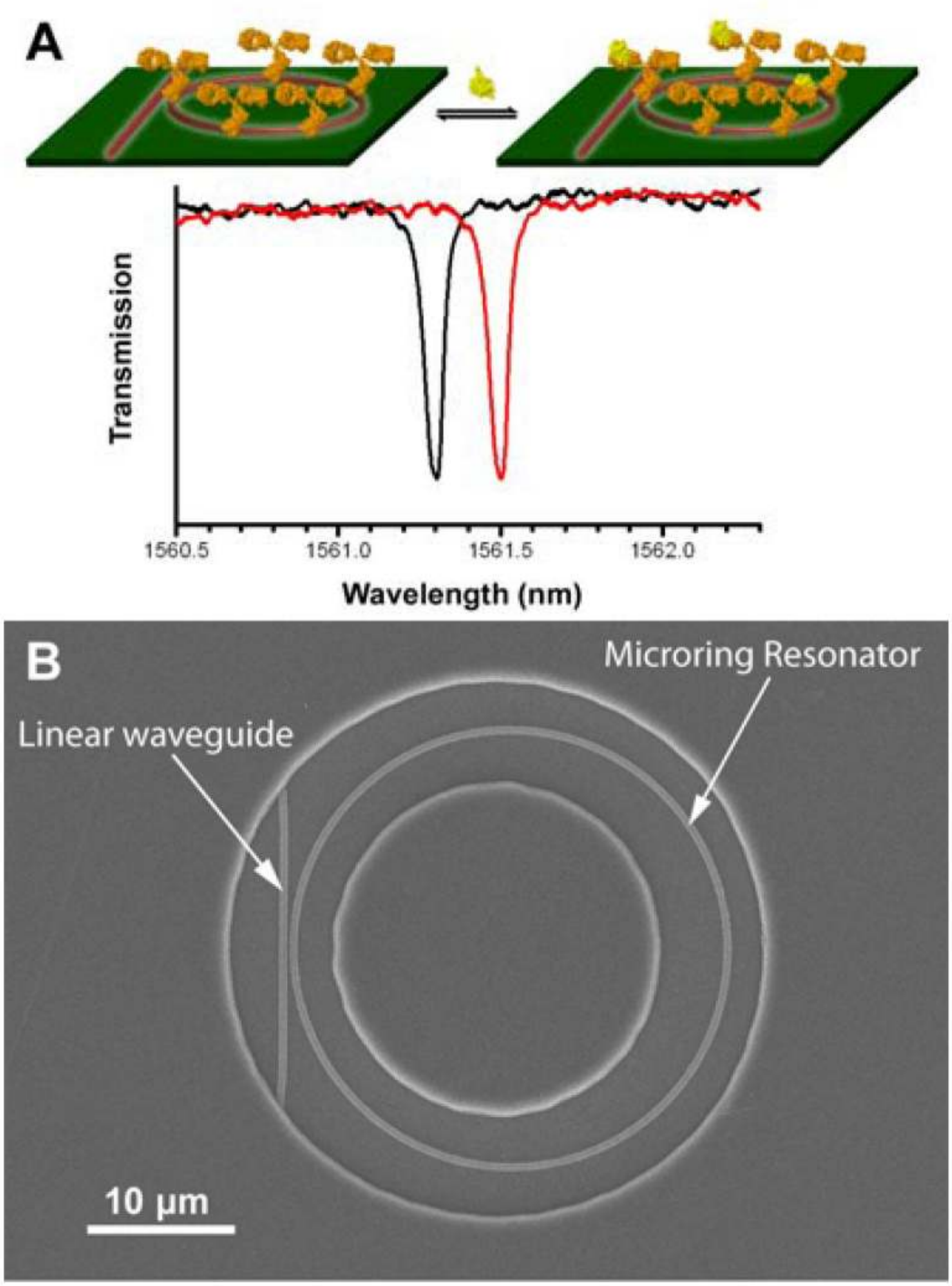

Figure 1.
(A) Schematic diagram illustrating the principle of microring optical resonator biosensing, including a representative transmission spectrum. (B) Top-view scanning electron micrograph image of a microring resonator and linear waveguide, visible through an annular opening in the fluoropolymer cladding layer.

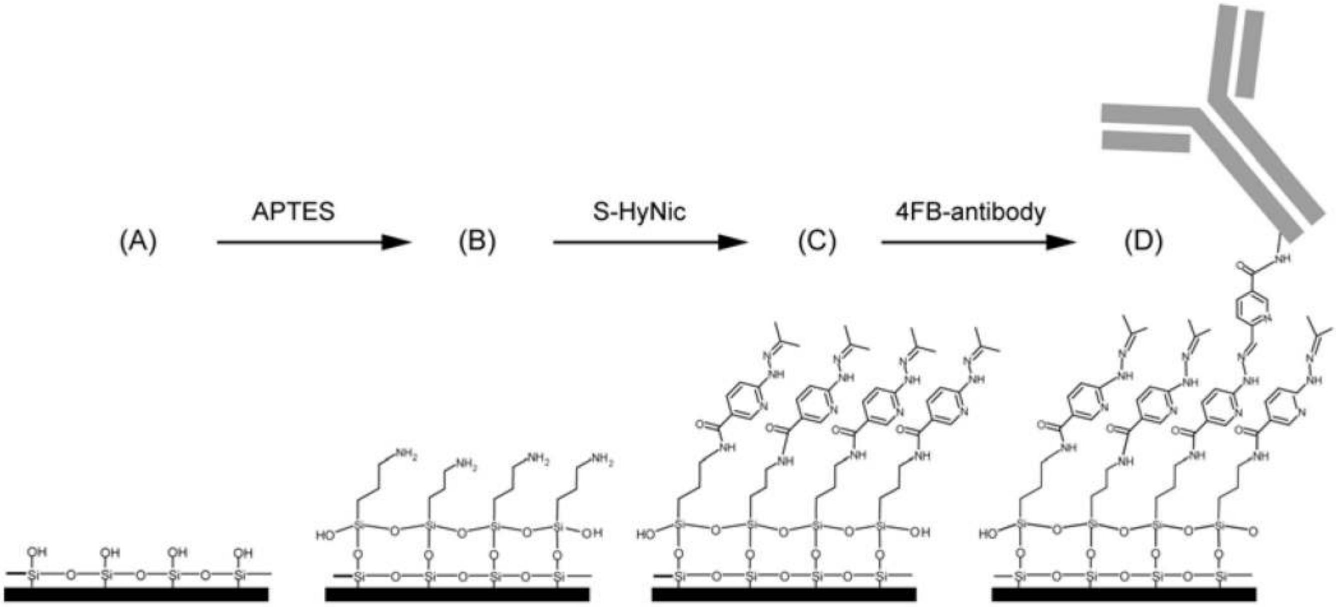

Figure 2.

Schematic showing surface functionalization. (A) Silicon surface of microring sensors prior to modification. (B) APTES reacts with the surface siloxane groups to generate an amino-terminated surface. (C) S-HyNic reacts with primary amines to create a HyNic-displaying surface. (D) Addition of 4FB-modified antibodies results in hydrazone bond formation between the 4FB moieties on the antibodies and the HyNic moieties on the surface.

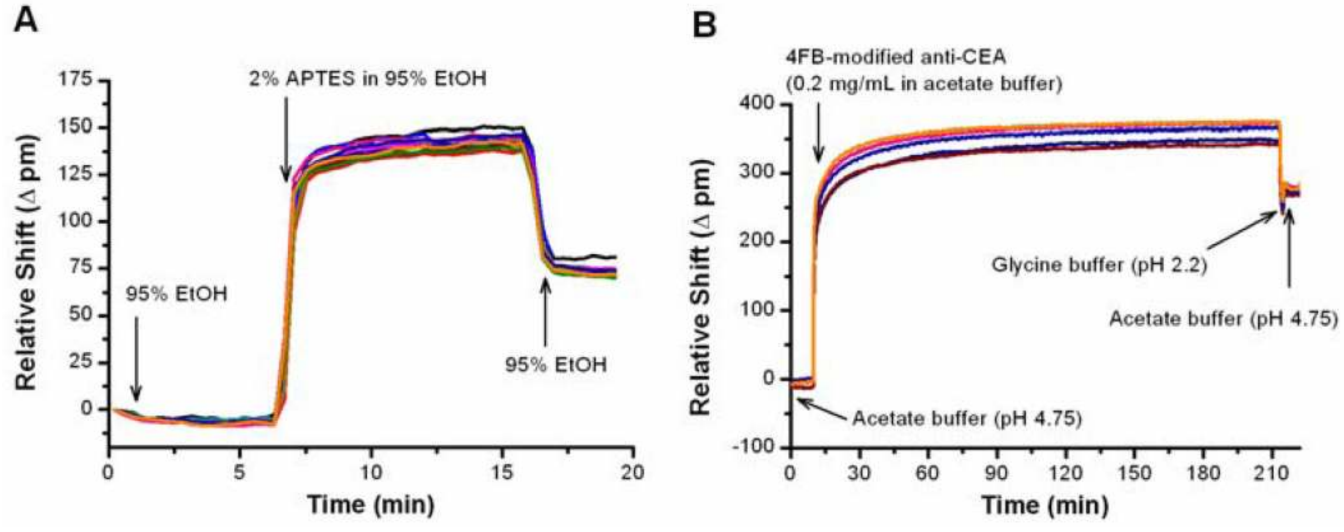

Figure 3.

(A) Real-time monitoring of the shift in resonance frequency for twelve microrings within the same sample flow chamber during organic modification via reaction with APTES. The microrings were initially submerged in 95% ethanol solution and a 2% solution of APTES injected at $t = 6.5$ min. The silane was flushed from the chamber and microrings returned to 95% ethanol after 10 min. **(B)** Real-time shift in resonance frequency from five individual microrings during covalent immobilization of antibody onto the sensor surfaces. The 4FB-tagged anti-CEA antibody was added at $t = 10$ min and removed (sample chamber returned to acetate buffer) at $t = 210$ min.

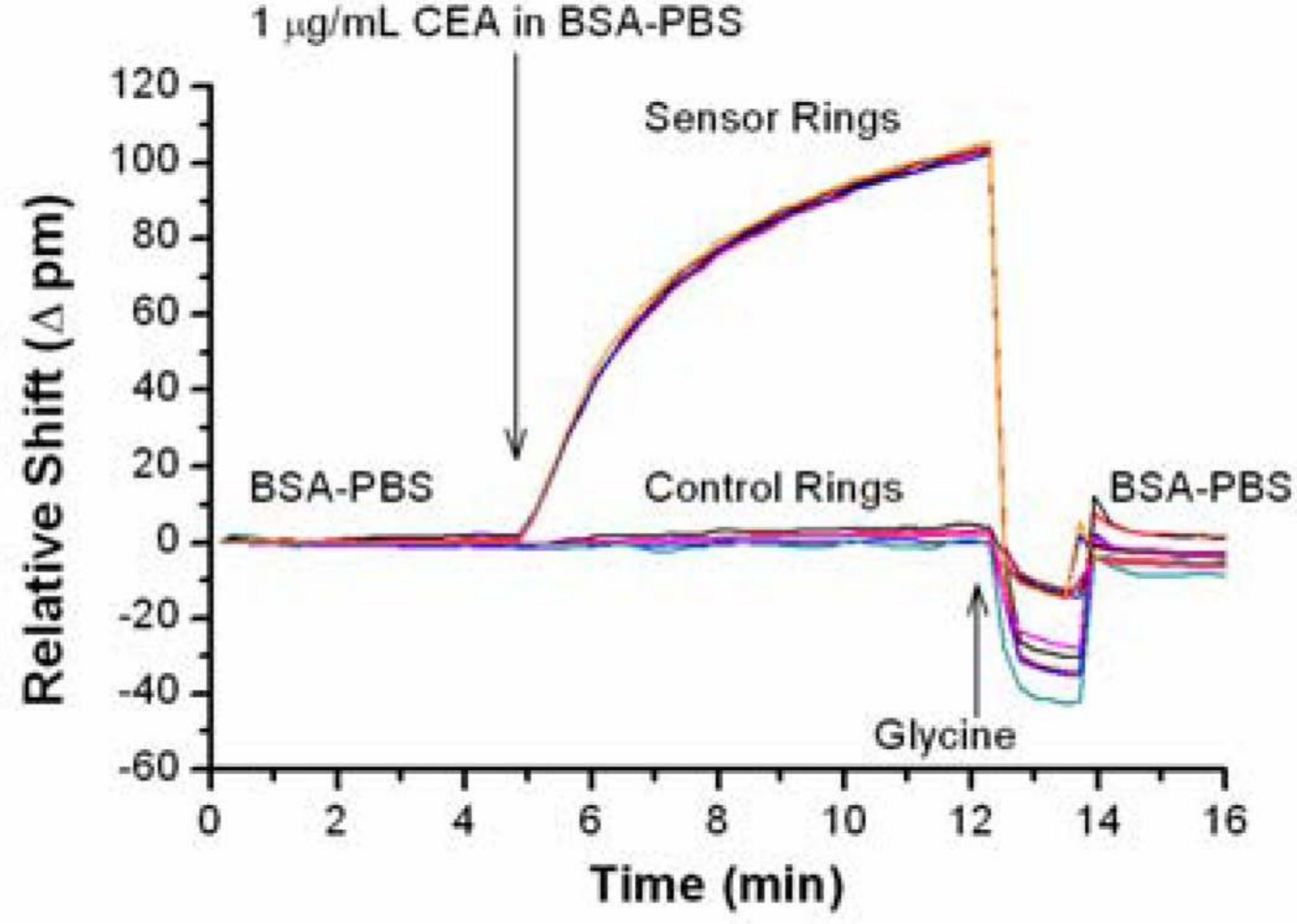

Figure 4.

Time-resolved detection of CEA using five anti-CEA-functionalized microrings alongside five control microrings that were not functionalized with antibody. Following exposure to CEA, the antibody surface was regenerated by exposure to glycine buffer for two minutes before returning to BSA-PBS.

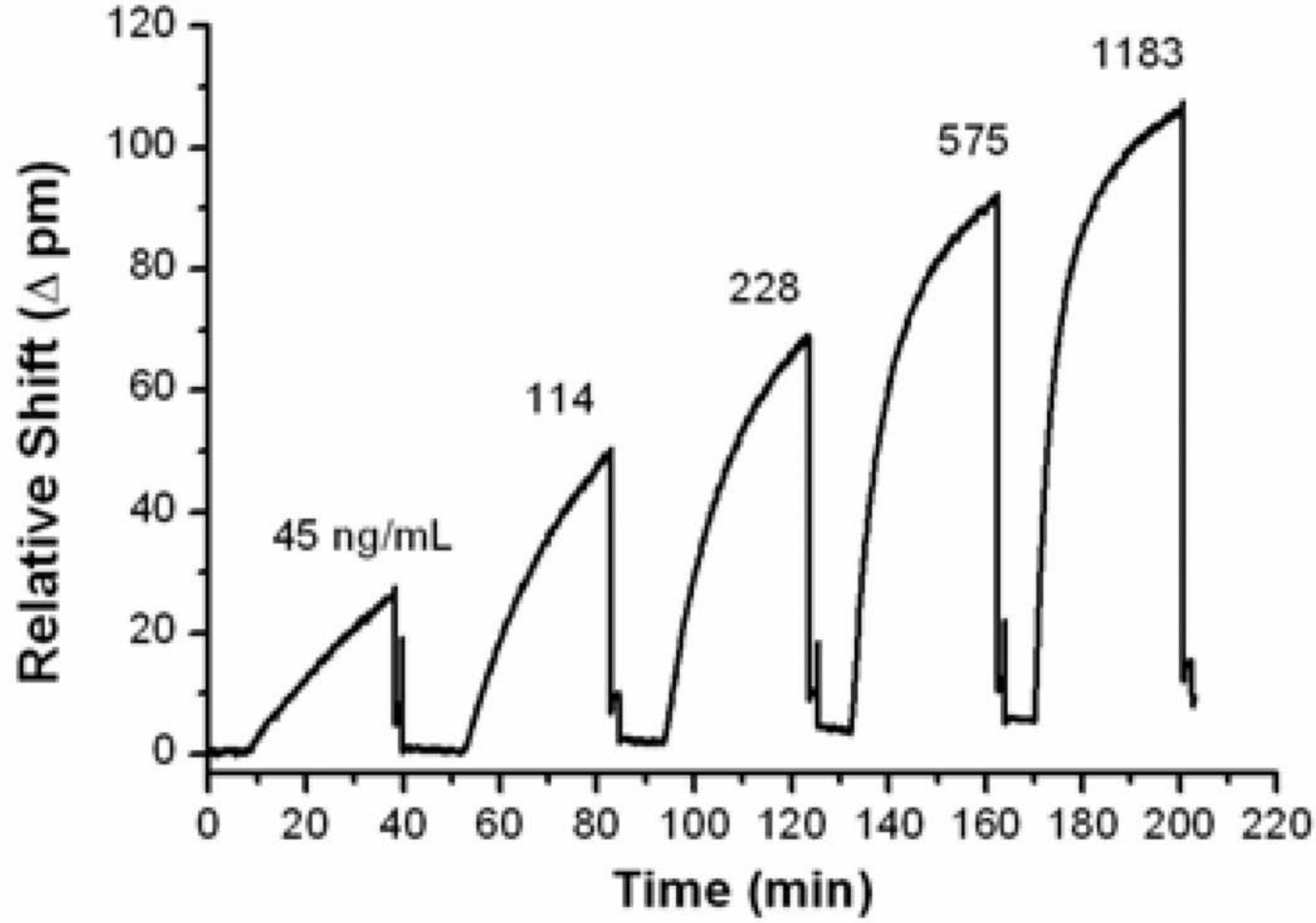

Figure 5.
Real-time monitoring of resonance frequency shifts of an anti-CEA antibody-functionalized microring upon exposure to increasing concentrations of CEA in BSA-PBS. After exposure to antigen, the antigen-antibody interaction was disrupted with glycine buffer, regenerating the original sensor surface, and the sample chamber was returned to BSA-PBS to reestablish the sensor baseline.

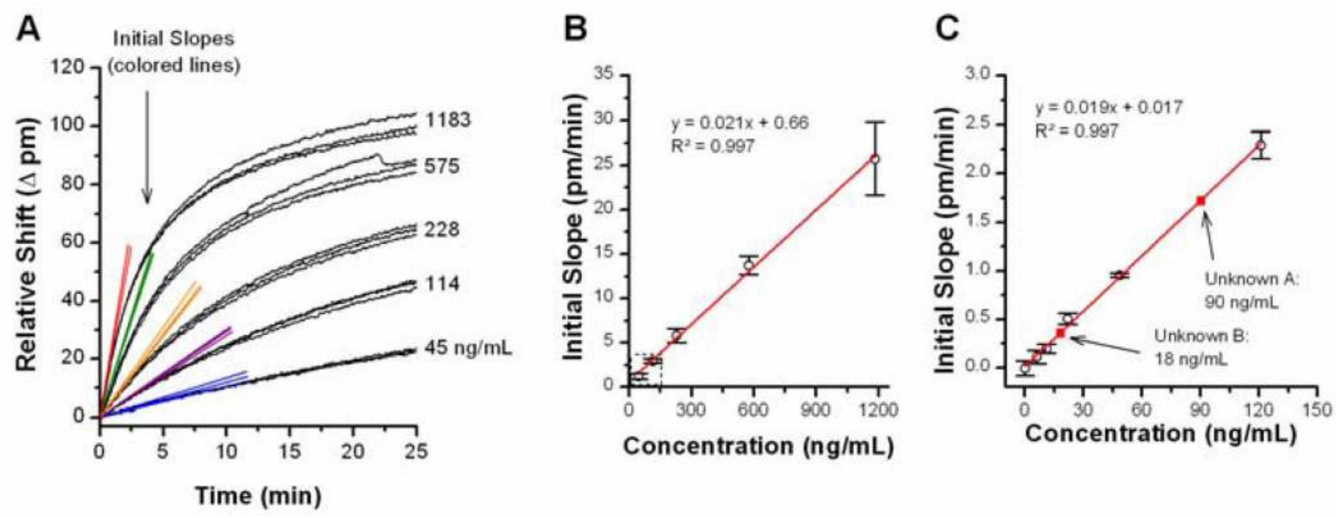

Figure 6.

Real-time, label-free detection of CEA using microring resonators. (A) Overlay of three time-resolved association curves for the same ring at each concentration of CEA. The colored traces are tangent lines to the association curve at *t* = 0 and are used to determine the initial slope of sensor response. (B) Concentration-response calibration plot of the initial slope of sensor response versus CEA concentration upon introduction of antigen standard solutions. The dashed box in the corner of the graph represents the range shown in panel (C) for measurement of CEA concentrations of unknown samples. (C) Overlay of the unknown solutions on a concentration-response calibration plot for CEA as determined by the initial slope method covering a dynamic range comparable to a commercial ELISA.

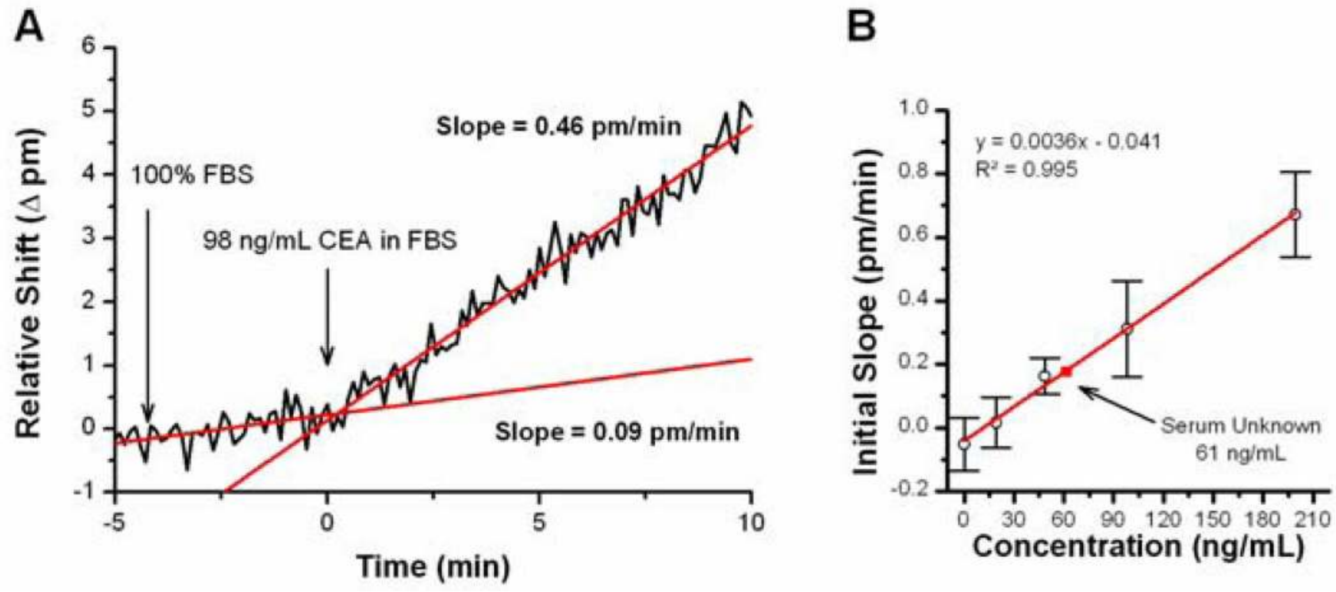

Figure 7.

(A) Example sensor response following addition of CEA in 100% FBS. Initial slope is determined by using a linear fit of the baseline to subtract the drifting baseline from the change in signal caused by addition of CEA in FBS. (B) Overlay of the unknown solution on the concentration-response calibration plot for CEA in 100% FBS. The concentration was determined to be 61 ± 23 ng/mL, which is in good agreement with a commercial ELISA assay.